The role of thermal spike compactness in radiation-induced disordering and Frenkel pair production in Ni[subscript 3]Al

Citation: Skirlo, S.A., and M.J. Demkowicz. "The Role of Thermal Spike Compactness in Radiation-Induced Disordering and Frenkel Pair Production in Ni[subscript 3]Al." Scripta Materialia 67, no. 7–8 (October 2012): 724–727.

As Published: http://dx.doi.org/10.1016/j.scriptamat.2012.06.029

Publisher: Elsevier

Persistent URL: http://hdl.handle.net/1721.1/101935

Version: Author's final manuscript: final author's manuscript post peer review, without publisher's formatting or copy editing

Elsevier Editorial System(tm) for Scripta Materialia
Manuscript Draft

Manuscript Number: SMM-12-1044R1

Title: The role of thermal spike compactness in radiation-induced disordering and Frenkel pair production in Ni3Al

Article Type: Regular Article

Keywords: molecular dynamics (MD), ordering, lattice defects, radiation

Corresponding Author: Mr. Scott Alexander Skirlo,

Corresponding Author's Institution: MIT

First Author: Scott Alexander Skirlo

Order of Authors: Scott Alexander Skirlo; Michael J Demkowicz, Ph.D. Mechanical Engineering

Abstract: We show that the shape of the kinetic energy distribution in radiation-induced thermal spikes may be described using a dimensionless number, proportional to (volume)^(2/3)/(surface area), known as compactness. The disorder produced in thermal spikes in Ni3Al increases with compactness because the thermal spike cooling rate, which determines the time available for thermal disordering, decreases with compactness. On the other hand, Frenkel pair production is inversely correlated to compactness because longer thermal spike lifetimes enhance vacancy-interstitial recombination.

The role of thermal spike compactness in radiation-induced disordering and Frenkel pair production in Ni_3Al

S. A. Skirlo[1], M.J. Demkowicz[2]

[1]Department of Physics, Massachusetts Institute of Technology, 77 Massachusetts Avenue, Cambridge, MA 02139

[2]Department of Materials Science and Engineering, Massachusetts Institute of Technology, 77 Massachusetts Avenue, Cambridge, MA 02139

We show that the shape of the kinetic energy distribution in radiation-induced thermal spikes may be described using a dimensionless number, proportional to $(\text{volume})^{2/3}/(\text{surface area})$, known as compactness. The disorder produced in thermal spikes in Ni_3Al increases with compactness because the thermal spike cooling rate, which determines the time available for thermal disordering, decreases with compactness. On the other hand, Frenkel pair production is inversely correlated to compactness because longer thermal spike lifetimes enhance vacancy-interstitial recombination.

Keywords: molecular dynamics (MD), ordering, lattice defects, radiation

Upon acquiring up to several tens of keV of kinetic energy from a collision with an incoming swift neutron or ion [1], an atom in a metal rapidly dissipates this energy to other nearby atoms, thereby initiating a thermal spike (TS) [2]. TSs are volumes on the order of ~10nm in diameter whose temperature reaches several thousand Kelvin for a few picoseconds. They have been extensively studied because of the important role they play in damage creation in materials under irradiation [3].

Atomistic modeling has been used to evaluate the dependence of defect creation rates on a broad range of TS parameters, such as ambient temperature, energy and direction of the primary knock-on atom (PKA) [4-7], crystal structure of the irradiated material [5], and overlap of multiple TSs [8]. However, in most analyses TS shape is assumed to be spherical and its influence on cascade damage is not addressed [9-13]. Here we show that the shape of TSs is typically non-spherical, that it may be quantified by a dimensionless parameter called “compactness,” and that it influences

defect production. These findings shed light on the mechanisms of disordering and Frenkel pair production under irradiation.

We conduct our investigation using molecular dynamics (MD) simulations of Ni_3Al: an $L1_2$-ordered intermetallic compound that disorders under heavy-ion irradiation [14]. In addition to vacancies, interstitials, and clusters thereof, TSs in Ni_3Al generate two species of antisites: one where an Al atom occupies a Ni site and another where a Ni atom occupies an Al site. Antisite creation in TSs accounts for radiation-induced disordering in Ni_3Al.

For this work, we have modified Mishin's EAM potential for Ni_3Al by joining it to the ZBL universal potential for short interatomic distances [15,16]. Polynomial splines were used to interpolate between the ZBL and EAM Ni-Al and Al-Al pairwise interaction terms over distances of 1 and 1.68 Å, and 1.7 and 2.35 Å, respectively. The intermediate distance behavior of the Ni-Ni pair potential (1.5-1.8 Å) did not spline well into the ZBL potential and was replaced with the intermediate distance curve from another Ni-Ni potential fitted to the Rose universal binding energy relation (UBER) by Mishin [17,18]. A spline from 0.5 and 1.5 Å connected this intermediate distance section to the ZBL potential at low interatomic distances and another spline from 1.8 and 2.2 Å connected this to the original Ni-Ni pair potential at large interatomic distances. All splines had 8 terms with degrees from 1 to -6. The modified potential correctly reproduced the pressure-volume data, equilibrium lattice parameters and cohesive energies of fcc Ni, fcc Al, and $L1_2$ Ni_3Al, as well as point defect formation energies reported in references [15,19]. In addition, cascades at each temperature reproduced defect counts compatible with the literature [12,13].

TSs were modeled in cubic simulation cells containing 500,000 atoms of $L1_2$ Ni_3Al equilibrated for 20 ps under periodic boundary conditions at temperatures of 100 K, 300 K, 600 K, and 900 K. Fifteen TSs were modeled at each temperature. TSs were initiated by sending a randomly selected PKA in a random direction with a kinetic energy of 10 keV. The system was then allowed to evolve under constant energy for 20-30 ps. Time steps were dynamically adjusted to ensure numerical accuracy and simulation efficiency.

To assess potential effects of microstructure, TS simulations were also performed at a 15° symmetric tilt grain boundary with a [001] tilt axis, constructed according to the method of Chen *et al.* [20]. TSs at this grain boundary tended to produce fewer Frenkel pairs, in agreement with previous studies [21-23], but otherwise did not differ noticeably from TSs in a perfect crystal.

TS chronology may be divided into two phases: ballistic and thermalized. Numerous high-energy interatomic collisions occur during the ballistic phase, which lasts only a few tenths of a picosecond and ends after the kinetic energy of atoms in the TS has fallen below the threshold energy required to create stable Frenkel pairs. Next, if the local temperature is high enough, the TS enters a thermalized, liquid state that resolidifies within about ten picoseconds [3]. Most of the antisites in irradiated Ni_3Al are created during the thermalized phase because the replacement collision sequence (RCS) mechanism, responsible for Frenkel pair generation during the ballistic phase, is very inefficient at producing antisites in Ni_3Al [11,24,25].

At the end of each simulation, defects were identified by comparing the final atomic structure to a perfect crystal reference. The nearest perfect crystal lattice site was found for every atom in the final structure. Depending on the type and number of atoms assigned to it, each perfect lattice site could be classified as defect-free, as a replacement (a new atom of the same type assigned), antisite (a different type of atom assigned), vacancy (no atom assigned) or interstitial (two atoms assigned). Similar methods were used elsewhere [26].

We use two independent methods to quantify the disorder produced by a TS: the number of antisites generated and the short range disorder (SRD) parameter. In a perfect $L1_2$ Ni_3Al crystal each Al atom has 12 Ni nearest neighbors, while in a randomly disordered crystal each Al has 9 Ni nearest neighbors on average. We define the SRD as

$$SRD = \sum_{i=0}^{n} \left(4 - \frac{Al_{Ni}^{i}}{3} \right) \qquad 1$$

where the sum is over all n Al atoms and Al_{Ni}^{i} is the number of Ni nearest neighbors for Al atom i. An Al atom with 12 Ni nearest neighbors does not contribute to SRD while an Al atom with 9 Ni nearest neighbors makes a unit contribution. The SRD parameter and the antisite number are independent ways of characterizing disorder: antisites quantify disorder relative to a reference lattice while SRD determines the local disorder around a given Al atom.

The shape of a TS was determined by characterizing its distribution of kinetic energy. We began by averaging the kinetic energy of every atom with those of all its nearest and next nearest neighbors. We define “volume atoms” as those with local average kinetic energies above a specified kinetic energy cutoff. As we will describe below, rather than fixing the same cutoff for all TSs, we

investigated how varying the number of volume atoms affected our characterization of TS shape, by selecting different cutoffs. Nearest neighbors of volume atoms that are not themselves volume atoms are termed "surface atoms." Using local average kinetic energies assures that transient fluctuations in kinetic energy do not lead to overestimates of the number of surface atoms.

Using the definitions above, we characterize TS shape by a dimensionless geometrical quantity called "compactness", C:

$$C = (36\pi)^{1/3} \frac{V^{2/3}}{S} \qquad 2$$

Here, S is the number of surface atoms and V the number of volume atoms. With the normalization given above, C=1 for a perfect sphere and is less than unity for all other shapes. For example, C=0.806 for a cube.

Figs 1.a) and 1.b) display C values for two representative TSs over a range of volumes and times. During the ballistic phase, which typically lasts 0.3-0.5ps, C varies markedly with both volume and time because kinetic energy redistribution occurs rapidly through binary collisions. In the thermalized phase, this form of energy redistribution is no longer possible. Instead, kinetic energy distributions gradually spread out by diffusion. Thus, during the first few picoseconds of the thermalized phase, the kinetic energy distribution retains a similar shape to that established in the ballistic phase.

For both examples in Fig. 1, C is nearly constant within a volume of 4000 to 7000 atoms and a time between 0.3 and 1.5 ps. This window is highlighted in blue in Fig. 1.a) and 1.b). At earlier times, C changes rapidly due to ballistic displacements while later the kinetic energy has become too dispersed to define a TS shape. Similarly for too large a volume, the kinetic energy distribution is determined by random thermal fluctuations outside the TS while too small a volume only picks out a small subset of the atoms that participate in a TS.

TS shape was characterized by the average of C over the volume window given above for one time slice between 0.3 and 1.5 ps. About 75% of antisites in Ni_3Al TSs are generated in this time window. Thus, the kinetic energy distribution in a TS has a definite shape—as characterized by compactness, C—during the period in which the majority of antisites are produced. Figs 1.c)-f)

visualize distributions of kinetic energies within this window as well as the final antisite distributions for the two representative TSs.

Compactness values for all the TSs we investigated fell within the range of 0.3 to 0.9, indicating that no TSs were perfectly spherical and some were markedly non-spherical. Our simulations also showed that the number of antisites produced in TSs increases with C. The relationship between C and antisite number is approximately linear with a slope that increases with ambient temperature, as shown in Fig 2. Assuming a zero intercept, 1.203T+476 gives the variation in slope with temperature. SRD shows the same qualitative correlation with C and bulk temperature as antisite number. Fig 3. shows that there is also a clear correlation between the number of vacancy-interstitial (Frenkel) pairs and C. Frenkel pair production, however, decreases with increasing ambient temperature and increasing C: exactly opposite of antisite production.

The results in Fig. 2 and 3 show that TS shape influences the production of radiation-induced defects. A possible reason for this is that TS shape affects TS cooling rate, which in turn affects the kinetics of defect creation or annihilation. To check this hypothesis, we calculated the decay time τ_{decay} over which the average temperature of TSs decreased from 3000K to 1200K. Average temperatures were determined for TS volumes of 7000 atoms: the same as in the C calculations. Fig 4. confirms that decay time indeed increases with both C and ambient temperature, T_A.

The dependence of decay time on C and T_A may be rationalized using a simple analytical model. If the liquid region in the TS is highly thermally conducting, then the temperature inside it remains approximately uniform. The cooling rate of the TS volume V is proportional to the difference in TS and ambient temperature as well as the TS surface area and may be expressed using Fourier's law,

$$cS\left(T - T_B\right) = \frac{3}{2} k_B \frac{dT}{dt} V \qquad 3$$

where c is a constant with dimensions of thermal diffusivity. Taking the T_A as constant, this equation is solved by an exponential decay:

$$T_{melt}\left(t\right) = T_A + \left[T_{melt}\left(0\right) - T_A\right] e^{-t/\tau} \qquad 4$$

where $T_{melt}(0)$ is the initial temperature of the molten TS core and

$$\tau = \frac{2Vk_B}{3Sc} = C\tau_0 \qquad 5$$

Thus, the characteristic time τ is proportional to compactness and a reference time τ_0, which is proportional to the cube root of the TS volume. The time that it takes the TS to go from 3000 K to 1200 K is the previously introduced decay time, τ_{decay} :

$$\tau_{decay} = C\tau_0 \ln\left(\frac{3000K - T_A}{1200K - T_A}\right) \qquad 6$$

If TS volume is approximately constant at a given T_A, then τ_{decay} increases with C and T_A, as observed.

Our findings shed light on the mechanisms of defect production under irradiation. There are two processes that affect disordering in TSs: thermal disordering, in which random mixing generates antisites, and vacancy mediated reordering, where migrating radiation-induced vacancies annihilate antisites to reduce free energy. These processes have been studied in many ordered alloys [27]. Several theoretical, computational, and experimental studies have attempted to correctly weigh the relative importance of each of these mechanisms in Ni_3Al [9-13,28,29]. The analytical models assumed that TS-affected regions become perfectly disordered during the ballistic phase and that subsequent vacancy reordering determines the final number of antisites. These models therefore predict that the volume of disordered regions decreases with increasing T_A because high T_A decreases TS quench rate, giving more time for vacancy reordering [9,10]. Atomistic simulations, however, arrived at the opposite result, bringing into question the importance of the vacancy reordering [12,13].

By contrast, if thermal disordering in the TS determines the final number of antisites, then we expect the number of antisites to increase with decay time. This is because the degree of thermal disordering depends on the time a TS spends at temperatures where disordering is significant. Fig. 2 confirms these expectations: antisite production increases with T_A and C because both increase τ_{decay}. Thus, our findings support the view that antisite production is governed by thermal disordering in TSs, not by vacancy-mediated reordering. Contrary to antisites, the number of Frenkel pairs decreases with increasing decay time because more time is available for

recombination [11]. Correspondingly, Fig. 3 shows that Frenkel pair production decreases with increasing C and T_A, i.e. with increasing τ_{decay}, as expected.

In summary, we have shown that the shape of thermal spikes (TSs) influences defect production during irradiation of Ni_3Al. Specifically, the compactness, C, of TS kinetic energy distributions is correlated to antisite and Frenkel pair production. This correlation is due to the longer decay times of more compact TSs, which extends the time spent at temperatures relevant to disordering and Frenkel pair annihilation. Antisite production increases with C, because more time is available for disordering, while Frenkel pair production decreases, because more time is available for recombination.

This work would not have been possible without the generous assistance of R. E. Baumer. MJD acknowledges discussions with M. L. Taheri and R. S. Averback.

References:

[1] R.E. Stoller, L.R. Greenwood, J. Nucl. Mater. 271 (1999) 57. doi:10.1016/S0022-3115(98)00730-2.

[2] F. Seitz, J.S. Koehler, Solid State Physics, ACADEMIC PRESS INC., New York, 1956.

[3] R.S. Averback, T.D. de la Rubia, Solid State Physics, Vol 51. 51 (1998) 281.

[4] D.J. Bacon, Y.N. Osetsky, Int. Mater. Rev. 47 (2002) 233. doi:10.1179/095066002225006575.

[5] D.J. Bacon, Y.N. Osetsky, R. Stoller, R.E. Voskoboinikov, J. Nucl. Mater. 323 (2003) 152. doi:10.1016/j.jnucmat.2003.08.002.

[6] R.E. Stoller, S.G. Guiriec, J. Nucl. Mater. 329 (2004) 1238. doi:10.1016/j.jnucmat.2004.04.288.

[7] R.E. Voskoboinikov, Y.N. Osetsky, D.J. Bacon, J. Nucl. Mater. 377 (2008) 385. doi:10.1016/j.jnucmat.2008.01.030.

[8] A.F. Calder, D.J. Bacon, A.V. Barashev, Y.N. Osetsky, Philos. Mag. 90 (2010) 863. doi:10.1080/14786430903117141.

[9] C. Abromeit, H. Wollenberger, J. Nucl. Mater. 191 (1992) 1092. doi:10.1016/0022-3115(92)90643-Y.

[10] C. Abromeit, H. Wollenberger, S. Matsumura, C. Kinoshita, J. Nucl. Mater. 276 (2000) 104. doi:10.1016/S0022-3115(99)00173-7.

[11] F. Gao, D. Bacon, Philos. Mag. A-Phys. Condens. Matter Struct. Defect Mech. Prop. 71 (1995) 43.

[12] F. Gao, D. Bacon, Microstructural Processes in Irradiated Materials. 540 (1999) 661.

[13] F. Gao, D. Bacon, Philos. Mag. A-Phys. Condens. Matter Struct. Defect Mech. Prop. 80 (2000) 1453.

[14] J. Eridon, L. Rehn, G. Was, Nucl. Instrum. Methods Phys. Res. Sect. B-Beam Interact. Mater. Atoms. 19-2 (1987) 626. doi:10.1016/S0168-583X(87)80126-X.

[15] Y. Mishin, Acta. Mat. . 52 (2004) 1451. doi:10.1016/j.actamat.2003.11.026.

[16] J.P. Biersack, J.F. Ziegler, Nucl. Instrum. Methods Phys. Res., 194 (1982) 93. doi:10.1016/0029-554X(82)90496-7.

[17] J.H. Rose, J.R. Smith, F. Guinea, J. Ferrante, Phys. Rev. B. 29 (1984) 2963. doi:10.1103/PhysRevB.29.2963.

[18] Y. Mishin, M.J. Mehl, D.A. Papaconstantopoulos, Phys. Rev. B. 65 (2002) 224114. doi:10.1103/PhysRevB.65.224114.

[19] R. Kinslow, High-Velocity Impact Phenomena, Academic Press, New York, 1970.

[20] S.P. Chen, D.J. Srolovitz, A.F. Voter, J. Mater. Res. 4 (1989) 62. doi:10.1557/JMR.1989.0062.

[21] M. Samaras, P.M. Derlet, H. Van Swygenhoven, M. Victoria, Phys. Rev. Lett. 88 (2002)

125505. doi:10.1103/PhysRevLett.88.125505.
[22] X. Bai, A.F. Voter, R.G. Hoagland, M. Nastasi, B.P. Uberuaga, Science. 327 (2010) 1631. doi:10.1126/science.1183723.
[23] M.J. Demkowicz, R.G. Hoagland, International Journal of Applied Mechanics. 1 (2009) 421. doi:10.1142/S1758825109000216.
[24] F. Gao, D. Bacon, Philos. Mag. A-Phys. Condens. Matter Struct. Defect Mech. Prop. 67 (1993) 289.
[25] F. Gao, D. Bacon, Philos. Mag. A-Phys. Condens. Matter Struct. Defect Mech. Prop. 71 (1995) 65.
[26] N. Doan, H. Tietze, Nucl. Instrum. Methods Phys. Res. Sect. B-Beam Interact. Mater. Atoms. 102 (1995) 58. doi:10.1016/0168-583X(94)00769-1.
[27] E.M. Schulson, J. Nucl. Mater. 83 (1979) 239
[28] M. Jenkins, P. Mavani, S. Muller, C. Abromeit, Microstructural Processes in Irradiated Materials. 540 (1999) 515.
[29] V.G. Kapinos, D.J. Bacon, Philos. Mag. A-Phys. Condens. Matter Struct. Defect Mech. Prop. 72 (1995) 1413.

Figure captions:

Figure 1. Comparison of two representative TSs at 900K: the left column is for a TS that generated 1080 antisites while the right had 1820 antisites. a) and b) show compactness, C, as a function of volume and time. The dark blue sections show the 4000-7000 atom window over which average C was computed for all TSs. c) and d) are final antisite distributions while e) and f) are kinetic energy distributions at times of 1.45 ps and 1.31 ps and a volume of 7500 atoms.

Figure 2. Antisite number (single species) vs. C for TSs at 100K, 300K, 600K, and 900K.

Figure 3. Frenkel pair number vs. C for 100K, 300K, 600K, and 900K TSs.

Figure 4. Decay time τ_{decay} vs. C for 100K, 300K, 600K, and 900K TSs.

Figure(s)

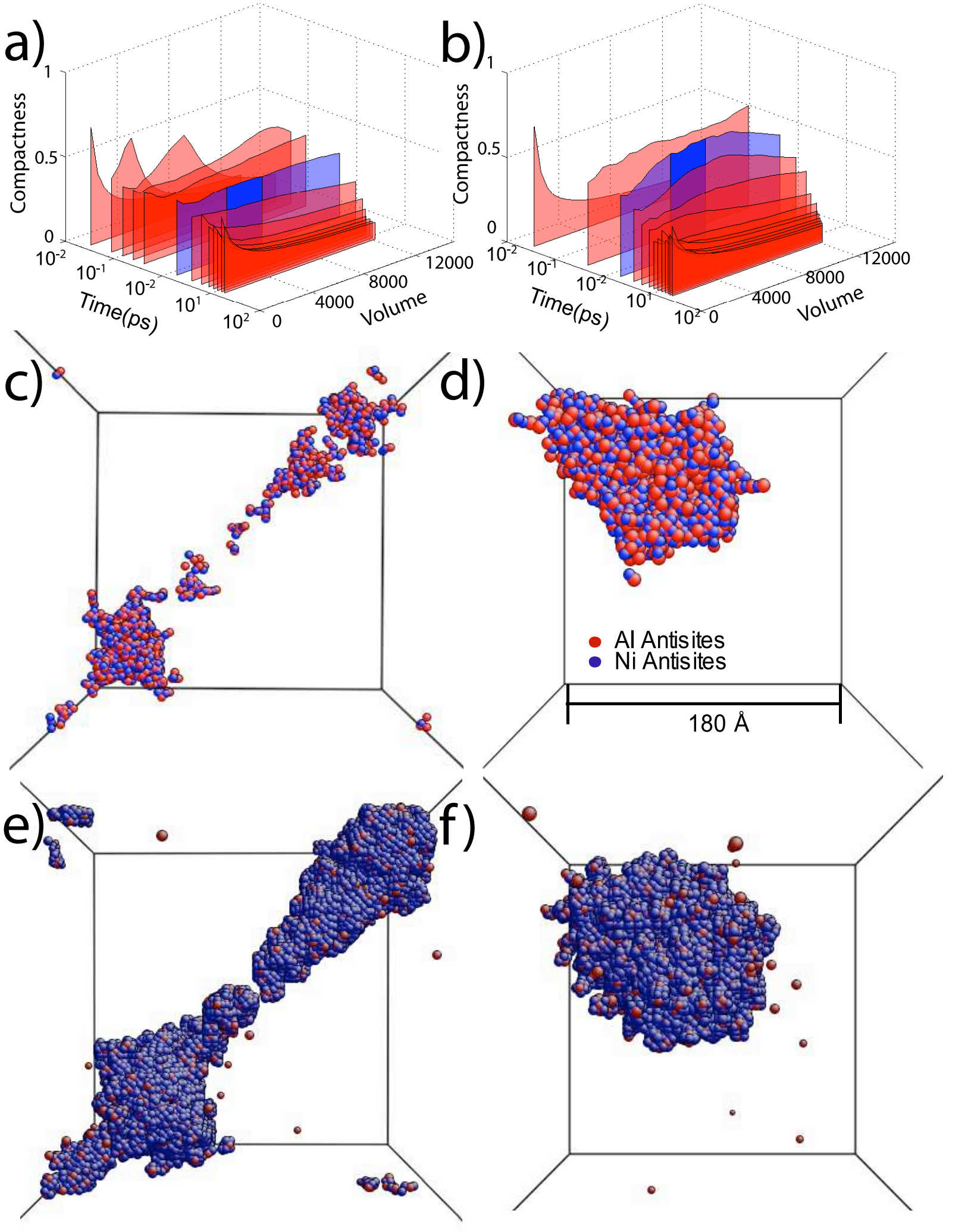
a)
b)
Compactness
1
0.5
0
10^{-2}
10^{-1}
10^{-2}
10^{1}
10^{2}
Time(ps)
0
4000
8000
12000
Volume
c)
d)
Al Antisites
Ni Antisites
180 Å
e)
f)

Figure(s)

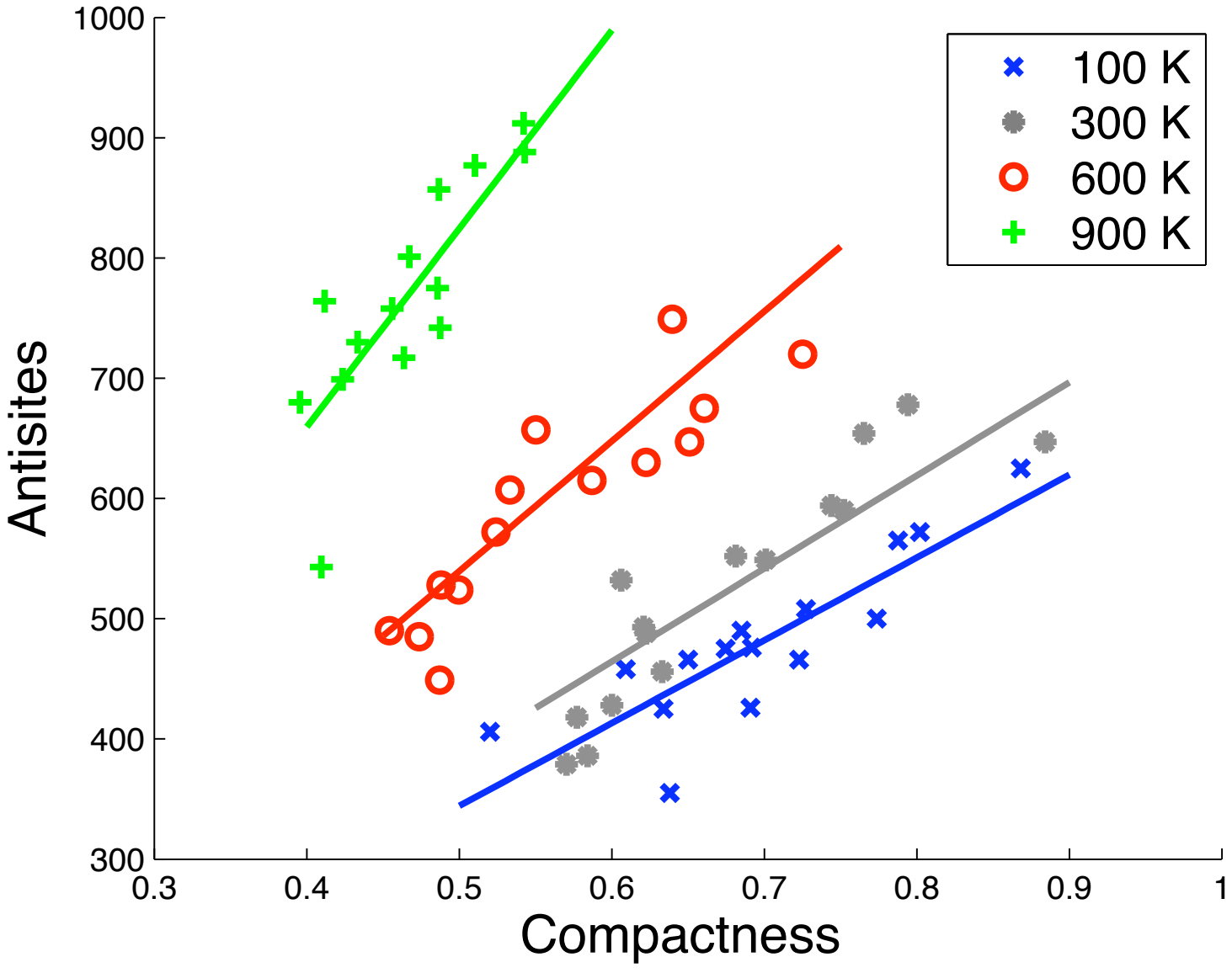
1000
900
800
700
600
500
400
300
Antisites
0.3
0.4
0.5
0.6
0.7
0.8
0.9
1
Compactness
100 K
300 K
600 K
900 K

Figure(s)

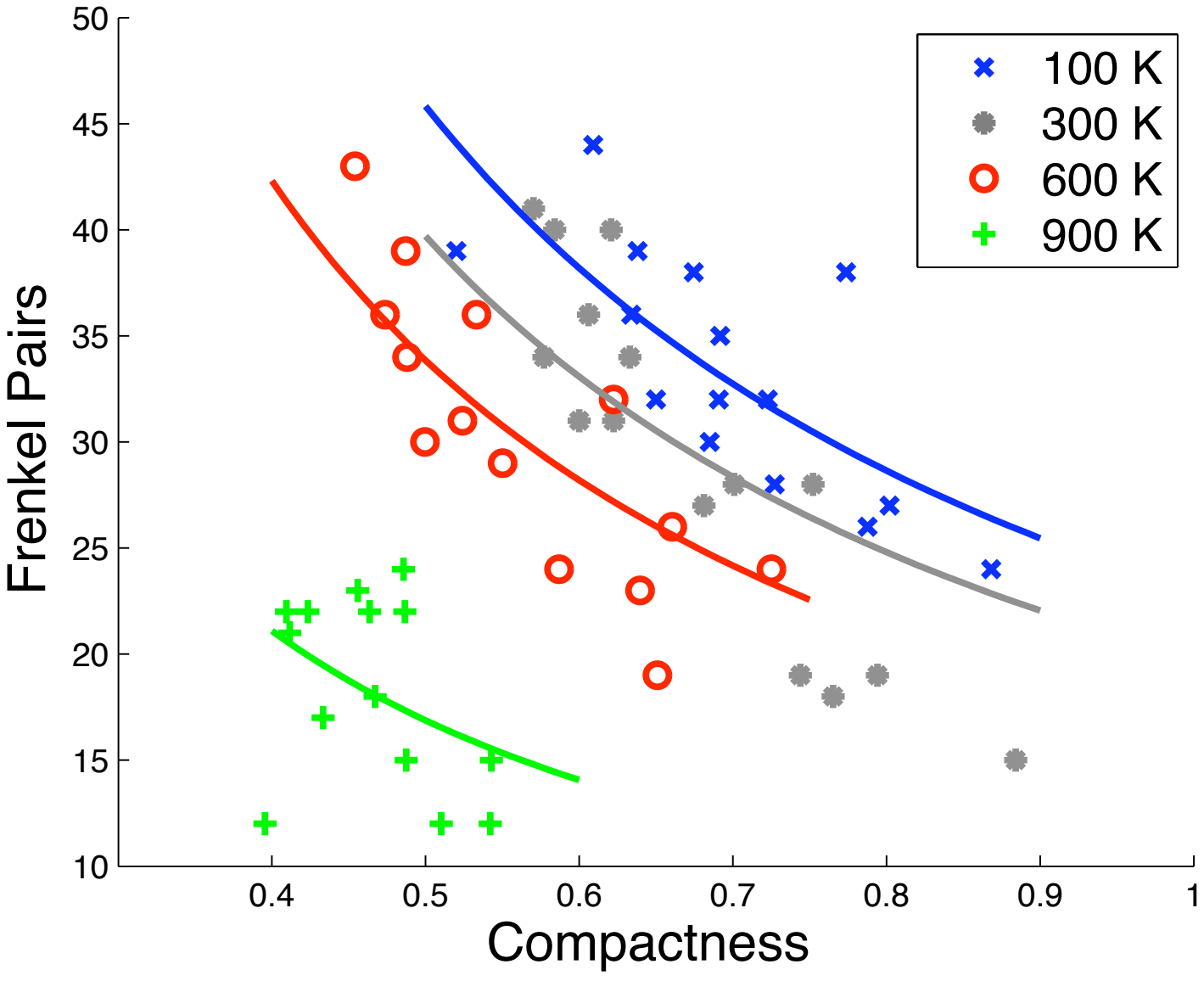
Frenkel Pairs
Compactness
50
45
40
35
30
25
20
15
10
0.4
0.5
0.6
0.7
0.8
0.9
1
100 K
300 K
600 K
900 K

Figure(s)

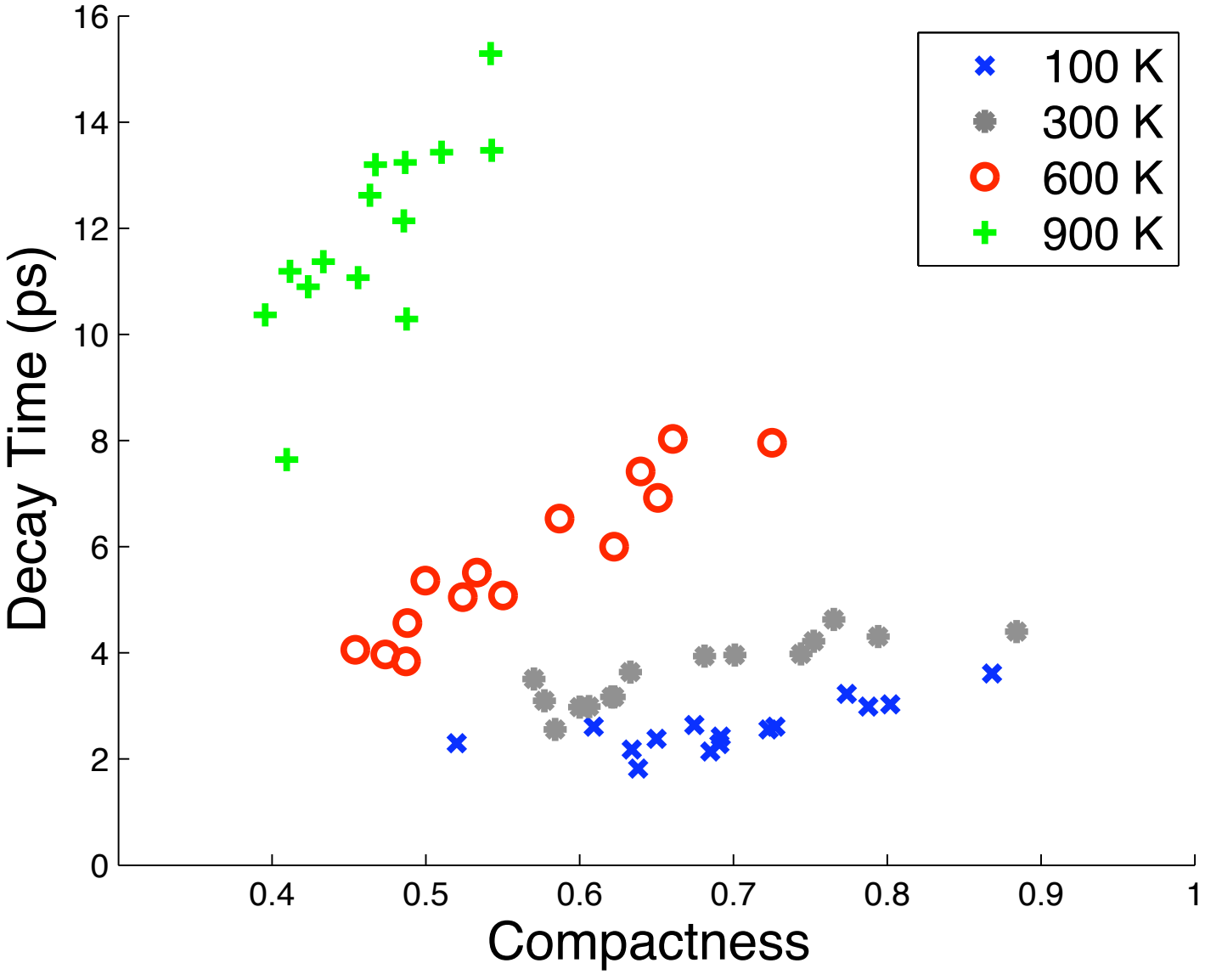
Decay Time (ps)
Compactness
100 K
300 K
600 K
900 K
0
2
4
6
8
10
12
14
16
0.4
0.5
0.6
0.7
0.8
0.9
1